# Small Angle Neutron Scattering Characterization of the Porous Structure of Carbons Prepared Using Inorganic Templates

Giselle Sandí,* P. Thiyagarajan,† Kathleen A. Carrado, and Randall E. Winans

*Chemistry and Intense Pulsed Neutron Source Divisions, Argonne National Laboratory, Argonne, Illinois 60439*

*Received May 7, 1998. Revised Manuscript Received November 19, 1998*

Small angle neutron scattering (SANS) was used for the characterization of the microstructure of carbons derived from organic-loaded inorganic template materials that are used as anodes in lithium ion cells. Pillared clays (PILC), layered silicates whose sheets have been permanently propped open by sets of thermally stable molecular props, were used as a template to load the organic precursors. Five organic precursors, namely pyrene, styrene, pyrene/trioxane copolymer, ethylene, and propylene, were used to load the PILC. Pyrolysis was carried out at 700 °C under nitrogen atmosphere. From SANS, information has been derived about the pore radius, mass fractal dimension, and the cutoff length (above which the fractal property breaks down) on each carbon. In general, the pore radius ranges from 4 to 11 Å, and the mass fractal dimension varies in the range from 2.5 to 2.9. Contrast-match SANS studies of carbons wetted in 84% deuterated toluene indicate that a significant amount of pores in carbon from pyrene are not accessible to the solvent, while most of the porous network of carbon from propylene is accessible.

## Introduction

As new applications demand higher energy and power storage, a rapid expansion of research on rechargeable batteries has occurred over the last 20 years.[1−3] The use of nonaqueous electrolytes allows for the utilization of lithium metal as the negative electrode. In this case, the mass and volume of the negative electrode can be very small in comparison to the positive electrode, which nearly doubles the specific capacity over that of the nickel−cadmium battery. However, the reactivity of lithium metal and the difficulty of plating and stripping it with high efficiency limit its use as an anode for secondary batteries. Carbonaceous materials have instead been used as anode electrodes, thus improving the safety and the efficiency of the battery.[4] In addition, the dendritic growth of metallic lithium upon charging can be avoided by using carbon anodes, prolonging the cycle life of a whole cell and improving the reliability. There is one drawback with a carbon anode: it may lower the specific energy density of a cell due to both a high reversible potential and a limited amount of lithium accommodation in the carbon matrix. These two factors vary with the type of carbon material. Thus far, carbon materials such as natural graphite, cokes, carbon fibers, nongraphitizable carbon, and pyrolitic carbon have been investigated,[5−9] but critical parameters such as surface area and porosity have not been quantified.

In our laboratories, disordered carbons with more predictable properties have been prepared using inorganic templates containing well-defined pore sizes.[10,11] We tested these carbons in electrochemical cells and found that they deliver high specific capacity (a measure of the power in mAh/g) and display excellent performance in terms of the number of cycles run.[12] Preliminary results have suggested that these carbons contain pores of comparable size to the templates from which they are derived, thus facilitating lithium ion diffusion. To understand the structure−function relationship in these carbons, we have applied small angle neutron scattering (SANS) to obtain information on their microstructure in terms of the pore size, the geometric arrangement of the pores in the carbonaceous matrix, and their accessibility to the solvent. Small-angle scattering from either X-rays or neutrons arises due to the

† Intense Pulsed Neutron Source Division.

* To whom correspondence should be addressed. Phone: (630) 252-1903. Fax: (630) 252−9288. E-mail: gsandi@anl.gov.

(1) Dahn, J. R.; Sligh, A. K.; Shi, H.; Way, B. W.; Weydanz, W. J.; Reimers, J. N.; Zhong, Q.; von Sacken, U. In *Lithium Batteries-New Materials, Developments and Perspectives*; Pistoia, G., Ed.; Elsevier: Amsterdam, 1994, p 1.

(2) Novak, P.; Muller, K.; Santhanam, K. S. V.; Hass, O. *Chem. Rev.* **1997**, *97*, 207.

(3) Owen, J. R. *Chem. Soc. Rev.* **1997**, *26*, 259.

(4) Fujimoto, H.; Mabuchi, A. Tokumitsi, K.; Kasuh, T. *J. Power Sources* **1995,** *54*, 440.

(5) Okuno, G.; Kobayakawa, K.; Sato, Y.; Kawai, T.; Yokoyama, A. *Denki Kagaku* **1994**, *65*, 226.

(6) Wilson, A. M.; Dahn, J. R. *J. Electrochem. Soc.* **1995**, *142*, 326.

(7) Takagi, R.; Okubo, T.; Sekine, K.; Takamura, T. *Denki Kagaku* **1997**, *65*, 333.

(8) Imanishi, N.; Kashiwagi, H.; Ichikawa, T.; Takeda, Y.; Yamamoto, O.; Inagaki, M. *J. Electrochem. Soc.* **1993**, *140*, 315.

(9) Schönfelder, H. H.; Kitoh, K.; Nemoto, H. *J. Power Sources* **1997**, *68*, 258.

(10) Sandí, G.; Winans, R. E.; Carrado, K. A. *J. Electrochem. Soc.* **1996,** *143*, L95.

(11) Sandí, G.; Carrado, K. A.; Winans, R. E.; Brenner, J. R.; Zajac,G. W. Mater. Res. Soc. Symp. Proc., *Macropor. Micropor. Mater.* **1996**, *431*, 39.

(12) Sandí, G.; Winans, R. E.; Carrado, K. A.; Johnson, C. S.; Thiyagarajan, P. *J. New Mater. Electrochem. Syst.***1998**, *1*, 83.

10.1021/cm980333j CCC: $18.00 
Published on Web 01/20/1999

presence of discontinuities in the density in a material. Thus, the particles and pores in the carbons can produce strong small angle scattering signals from X-rays (SAXS) or neutrons (SANS) in a wide momentum-transfer ($q = 4\pi \sin\theta/\lambda$ where $2\theta$ is the scattering angle and $\lambda$ is the wavelength of radiation) range. The small angle scattering data can be modeled to obtain information on the microstructure of the porous network. We used SANS in the present study, as neutrons offer an additional advantage over X-rays in being able to suppress the scattering contribution from the carbon particles to allow the investigation of the closed porosity in these carbons. This is accomplished by soaking the carbon powders in organic solvent (a mixture of appropriate volume fractions of normal and deuterated solvents) whose neutron scattering length density is identical to that of the carbon matrix. This constitutes a contrast-match SANS experiment. From this technique it is possible to learn whether all the pores in the network are accessible to the solvent and to characterize the microstructure of those pores which are not accessible to solvent ("closed pores"). We performed contrast-match SANS on carbons derived from pyrene and propylene, which represent both closed-pore and open-pore systems, respectively.

## Experimental Section

The synthesis of the pyrolyzed pillared clays (PILCs) using different organic precursors (pyrene, styrene, trioxane/pyrene, ethylene, and propylene) has been reported.[10−12] The carbon derived from pyrene and styrene exists as small flakes, while that from propylene, ethylene, and trioxane is powdery. For the SANS measurements the carbons derived from all the organic precursors were ground to a powder prior to loading in the sample containers. SANS of dry powders of carbons in Suprasil cells (path length = 1 mm) were measured with a time-of-flight SANS instrument, SAD at the Intense Pulsed Neutron Source at Argonne National Laboratory.[13] SAD uses neutrons from a solid $CH_4$ moderator at 24 K with a wavelength from 0.5 to 14 Å, binned into 67 wavelength channels with 5% wavelength spread in each channel. The scattered neutrons are detected by a 20 × 20 $cm^2$ $^3$He area detector with 64 × 64 spatial channels. This instrument provides data in a $q$ range of 0.005−0.35 $Å^{-1}$ in a single measurement. For the contrast-variation SANS study, carbons from pyrene and propylene were measured as slurries in toluene (0, 25, 50, 75, and 100% toluene-*d*) in 1 mm path length Suprasil cells. For the slurries, the powders were slowly evacuated to avoid air bubble formation prior to adding the solvent. The scattering from an empty cell was used for background correction for the powder samples, and the corresponding solvent of appropriate volume not occupied by the carbon was used as the background for the samples soaked in the solvent. All other routine corrections[14] were carried out prior to the analysis.

For comparison with SANS data, $N_2$ BET surface areas and pore size distributions were obtained on an Autosorb 6 instrument from QuantaChrome. Approximately 0.10 g of material was weighed into a Pyrex tube and evacuated at 80 mTorr overnight at room temperature. After back filling with He, the carbon was only briefly exposed to air prior to analysis. The static physisorption experiments consisted of determining the amount of liquid nitrogen adsorbed or desorbed from the material as a function of pressure ($P/P_o$ = 0.025−0.999, in increments of 0.025).

(13) Thiyagarajan, P.; Epperson, J. E.; Crawford, R. K.; Carpenter, J. M.; Klippert, T. E.; Wozniak, D. G. *J. Appl. Crystallogr.* **1997**, *30*, 280.

(14) Copley, J. R. D. *J. Appl. Crystallogr.* **1988**, *21*, 639.

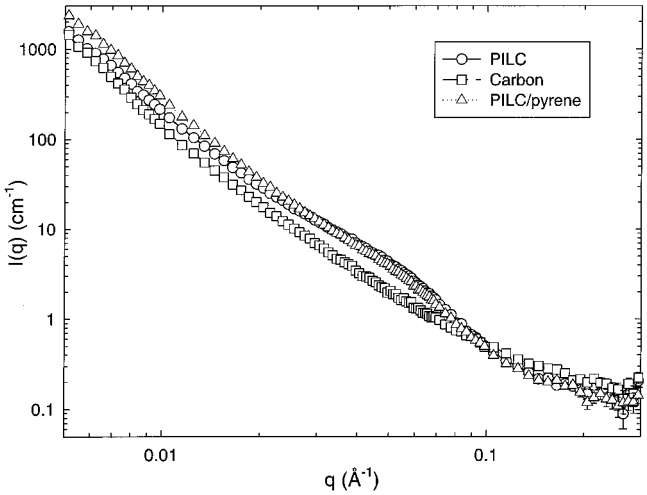


**Figure 1.** Plot of log $I$ vs log $q$ of the SANS for PILC, PILC/pyrene composite, and carbon, as described in the inset.

## Results and Discussion

Figure 1 shows a log−log plot of the intensity of the scattered neutrons [$I(q)$] and the magnitude of the momentum transfer ($q$) for PILC, PILC loaded with pyrene prior to pyrolysis, and the carbon obtained after pyrolysis at 700 °C and after removal of the clay matrix. The scattering curves are nearly identical for the PILC and the organic loaded clay, indicating that there is no appreciable structural change in the pillared clay upon organic incorporation. Both the pillared clay and the loaded pillared clay exhibit a hump in the $0.02 < q < 0.08$ $Å^{-1}$ region, suggesting the presence of some aggregates. On the other hand, the scattering data for the pyrolyzed carbon sample does not show such a hump. Another interesting feature in Figure 1 is that all the samples show a power-law scattering in $0.005 < q < 0.05$ Å, but the scattering intensity from the pyrolyzed carbon sample is larger in the high $q$ region than that for the PILC samples. This implies that the hydrocarbons originally present in the PILC produced voids in the carbon network upon pyrolysis and the increased scattering in the high $q$ may be due to small pores in the carbon network. Similar features are seen in the SANS data for all the PILC samples loaded with styrene, trioxane, propylene, and ethylene and will be discussed later.

In addition to X-ray powder diffraction measurements of the carbons that show a very broad 002 peak,[11] the Lc values (layer dimension perpendicular to the basal plane) calculated from this peak as described by Kinoshita[15] are in the range from 15 to 18 Å, which indicate that the carbon particles are composed of a spherical assemblage of many quasigraphitic crystallites. Furthermore, the Lc values are comparable to those of the disordered carbons heated at temperatures higher than 1500 °C.[15] To better understand the microstructure of the carbons, it is essential to have a well-characterized inorganic template to begin with. For PILC templates, a <2 $\mu$m clay fraction is suspended in $[Al_{13}O_4{\cdot}(OH)_{12}(H_2O)_{24}]^{7+}$ pillaring ions. Upon calcination at 400 °C, water and hydroxyl molecules are removed

(15) Kinoshita, K. *Carbon, Electrochemical and Physicochemical Properties*; John Wiley & Sons: New York, 1988; p 32.

and $Al_2O_3$ species bind to the intracrystal surfaces of the clay, acting as pillars.

To gain a better understanding of the microstructure of these complex systems, we used the theory of Sinha et al.[16] and Teixiera,[17] developed for the description of the network structure of aggregated silica particles. For porous materials, the mass will scale as:

$$M(r) \propto r^{D} \tag{1}$$

where the $D$ is the mass fractal dimension that can have a noninteger value less than 3. It describes how the mass of the cluster increases with its linear dimension, $r$. While a material may appear perfectly regular and three-dimensional on the scale of a centimeter it may scale in a fractal manner on the nanometer scale. Scattering experiments probe the density correlations on length scales that correspond to the inverse momentum transfer, and since the intensity per particle scales with the correlated mass in the probing volume, it is expected that the intensity scales as $q^{-D}$. The scattering behavior exhibited by fractal materials can be used to gain insight into the physical structure of these samples. For instance, a smaller fractal dimension signifies an open structure and dense materials will have a value close to 3.

According to Sinha et al.[16] and Teixiera,[17] the scattering intensity $I(q)$ measured for a network can be expressed as a product of the form factor of the spherical particle, $P(q)$, and the interparticle structure factor, $S(q)$

$$I(q) = \Phi V^2(\rho_P - \rho_0)^2 P(q) S(q) \tag{2}$$

where

$$P(q) = \left[3\frac{\sin(qr) - qr\cos(qr)}{(qr)^3}\right]^2 \tag{3}$$

and

$$S(q) = 1 + \frac{1}{(qr)^D}\frac{D\Gamma(D-1)}{\left(1+\frac{1}{q^2\xi^2}\right)^{(D-1)/2}}\sin[(D-1)\arctan(q\xi)] \tag{4}$$

In eq 2, $\Phi$ and $V$ are the concentration and volume of the scatterers, and $\rho_P$ and $\rho_0$ are the scattering length densities (defined later) of the particle and the network matrix, respectively. In eq 3, $r$ is the radius of the spherical particle. The difference between the scattering length densities of the matrix and the scatterer is known as the contrast, and if they are equal there will not be any coherent scattering. In eq 4, $D$ is the mass fractal dimension, $\xi$ is the cutoff length above which the density of the fractal object will approach the macroscopic density, and $\Gamma$ is a gamma function.

Our justification to use the theory of Sinha et al.[16] and Teixiera[17] for the analysis of the scattering data from the porous carbons is based on Babinet's theorem described by Porod.[18] According to this, scattering techniques cannot distinguish between systems with particles in a matrix and voids in a matrix. Freltoft[19] used Sinha's approach in their model and treats the scattering data in the high $q$ end to be due to a fundamental silica particle and that from the intermediate $q$ range to be due to the silica network which consists of silica and the voids. The low $q$ data corresponds to the silica particles of a given macroscopic density. We believe that this model should be equally applicable to the porous carbons considered here. The data in the high $q$ region should represent the morphology of the small pores and that in the middle $q$ region correspond to the density variation represented by the mass fractal dimension. Another important feature of this model is that it provides reasonable structural parameters for the size of the fundamental particle and the mass fractal dimension, even when the measured data do not contain data in the low $q$ region to access the cutoff length.[19,20]

Equations 2, 3, and 4 were used to fit the $I(q)$ data for the carbon powder to obtain $r$, $\xi$, $D$ and a prefactor which includes the volume and the contrast factors. For the carbons, $V$ and $r$ are the volume and the radius of the spherical pore and $\rho_P$ and $\rho_0$ are the scattering length densities of the pore and the carbon network, respectively. Nonlinear least-squares fitting of the data was done by using the routines available in Igor Pro 3.13 package, and the experimental errors in $I(q)$ at each $q$ were used as weighting factors.

Fitting of the SANS data for PILC in Figure 1 using eq 2 gave an $r$ value of $3.7 \pm 0.3$ Å that is close to the size of 5.0 Å reported by Bergaoui et al.[21] for unhydrated $[Al_{13}O_4(OH)_{12}]^{7+}$ ions, which indicates the validity of the model.

Figure 2 shows SANS data for four carbons derived from PILC and different organic precursors. The solid curves shown in each plot are actual fits to eq 2 for the measured data. Table 1 collects the parameters of the radius of the pore, the mass fractal dimension, and the cutoff length derived from these fits. The mass fractal dimensions for the carbons are slightly larger than that determined for the PILC, indicating that some densification has occurred in the carbon matrix. It can be seen in this table that the average pore radius varies in a range from 4 to 11 Å for the carbons. The pore radii are larger for the carbons from pyrene and styrene than those for carbons derived from ethylene and propylene. We believe that this difference in carbon pore size may be related to the number of molecules that can interact with an $Al_2O_3$ pillar in the intracrystalline PILC void space. Also, the accessibility to the pillars of the organic molecules may be limited by their molecular size. Thus, the bulky pyrene and styrene molecules cannot easily approach the pillars, while the linear compounds propylene and ethylene can diffuse to the pillars more

(16) Sinha, S. K.; Freltoft, T.; Kjems, J. K. In *Kinetics of Aggregation and Gelation*, Family, F.; Landau, D. P., Eds.; Elsevier Sciences: Amsterdam, 1984, p 87.

(17) Teixiera, J. In *On Growth and Form: Fractal and Non-Fractal Patterns in Physics*; Stanley, H. E., Ostrowsky, N., Eds.; Martinus Nijhoff: Dordrecht, 1986; p 145.

(18) Porod, G. In *Small Angle X-ray Scattering*; Glatter, O., Kratky O., Eds.; Academic Press: New York, 1982; p 43.

(19) Freltoft, T.; Kjems, J. K.; Sinha, S. K. *Phys.Rev. B* **1986**, *33*, 269.

(20) Loong, C. K.; Thiyagarajan, P.; Richardson J. W., Jr.; Ozawa, M; Suzuki, S. *J. Catalysis* **1997**, *171*, 498.

(21) Bergaoui, L.; Lambert, J. F.; Vicente-Rodríguez, M. A.; Michot, L. J.; Villiéras, F. *Langmuir* **1995**, *11*, 2849.

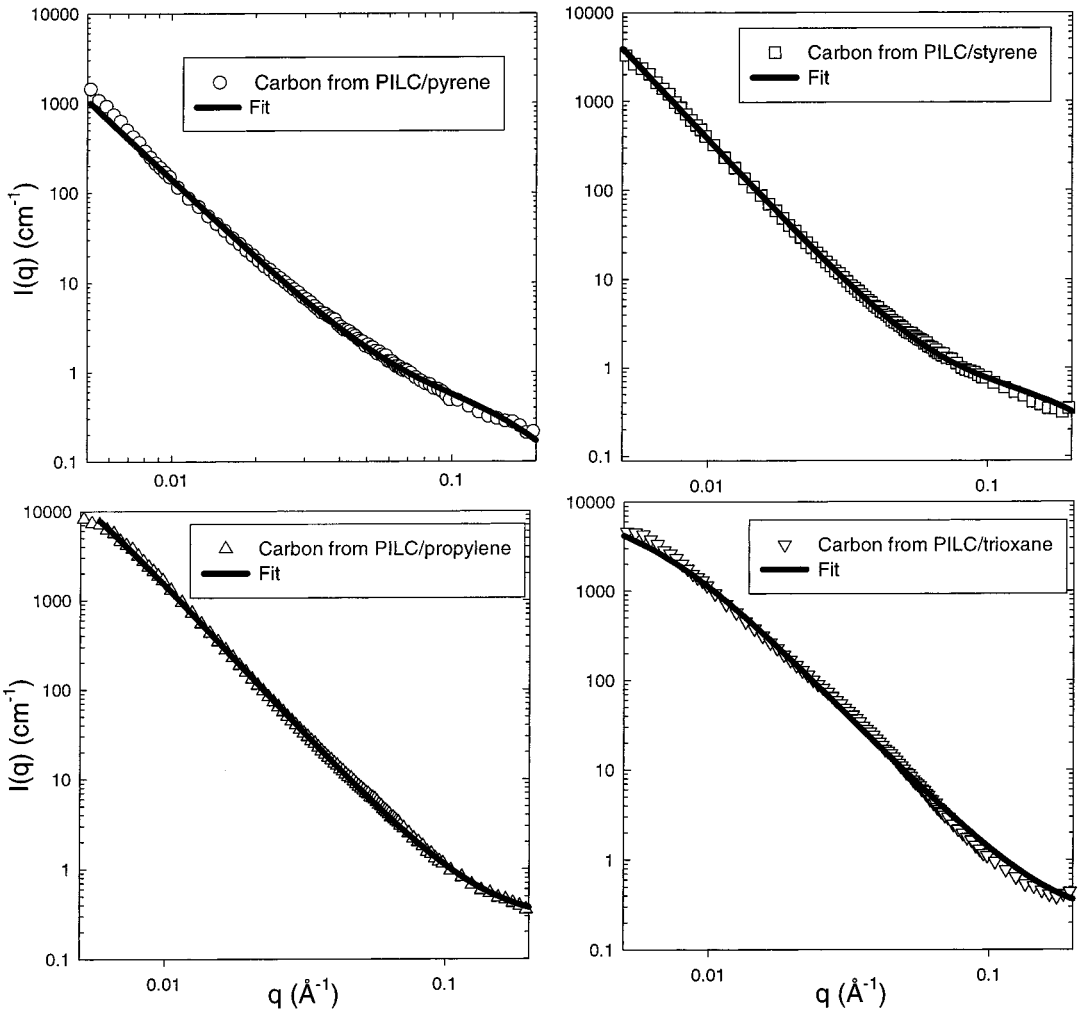


**Figure 2.** Plot of log $I$ vs log $q$ of the SANS for carbon derived from PILC/pyrene, PILC/styrene, PILC/trioxane/pyrene, and PILC/propylene, as described in the inset. The solid lines represent the fits to the data.

**Table 1. Experimental Parameters Calculated from the Fits to SANS Data Using Eq 2[a]**

| sample | $r$ (Å) | $\xi$ (Å) | $D$ |
|---|---|---|---|
| PILC | 3.7 ± 0.3 | 876 ± 400 | 2.47 ± 0.01 |
| carbon from PILC/pyrene | 11.4 ± 0.3 | 1380 ± 320 | 2.68 ± 0.02 |
| carbon from PILC/styrene | 10.9 ± 0.2 | 806 ± 54 | 2.88 ± 0.01 |
| carbon from PILC/ethylene | 4.0 ± 0.6 | 112 ± 0.6 | 2.74 ± 0.02 |
| carbon from PILC/propylene | 4.0 ± 0.1 | 364 ± 4 | 2.86 ± 0.01 |
| carbon from PILC/trioxane | 2.3 ± 0.4 | 161 ± 1 | 2.77 ± 0.01 |

[a] $r$ = pore radius. $\xi$ = cutoff length. $D$ = fractal dimension.

efficiently. The percentage organic loading in the pillared clay, calculated by thermal gravimetric analysis, follows the trend pyrene < styrene < ethylene = propylene. Figure 3 shows a possible schematic representation of the structure, including pores, of the carbons derived from the aromatic hydrocarbons. The carbonization process is catalyzed by the acidic sites of the clay (especially those on the pillars), allowing for pyrolysis at temperatures lower than usually needed.[22] The distance between pillars corresponds to about 15 Å, as described by Shabtai et al.[23] Since $r$ for PILC prior to loading and pyrolysis is 3.70 Å, it is expected that $r$ of the carbon derived from pyrene (pores and voids)

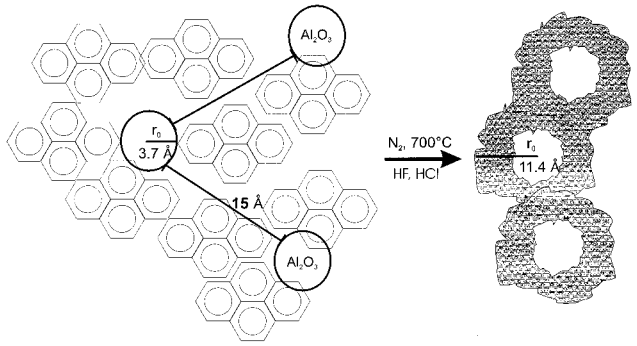


**Figure 3.** Schematic representation of the mechanism of formation of porous carbon using pillared clays as templates and pyrene as the carbon precursor. The average pore size $\rho_0$ is about 11 Å for this carbon.

should have a value of 11.3 Å. The $r$ value obtained by SANS for this carbon was 11.4 Å, in excellent agreement with the expected value. This also indicates that the pyrene molecules are homogeneously dispersed between the pillars in the clay, filling the space created by the pillaring process. For the other carbons the $r$ value is smaller than predicted, which implies that the carbon forms thin shells around the pores. This is in agreement with the percentage yield of the carbon, as previously described.

(22) Balaban, A.; Nenitzescu, T. In *Friedel–Crafts Chemistry*; Olah, G., Ed.; Wiley: New York, 1973; Vol. 2, p 979.
(23) Shabtai, J.; Rosell, M.; Tokarz, M. *Clays Clay Miner.* **1984**, *32*, 99.

Contrast variation SANS measurements were performed on carbons from pyrene and propylene by using a mixture of normal and deuterated toluene at deuteration levels of 0, 25, 50, 75, and 100%. The scattering length density values of toluene and toluene-$d_8$ are 0.94 $\times$ $10^{10}$ and 5.64 $\times$ $10^{10}$ cm$^{-2}$ , respectively. This is calculated by using

$$\rho = \frac{\sum b}{\sum M} d N_A \qquad (5)$$

where $b$ and $M$ are the scattering length and the atomic weight of individual atoms in the molecule, $d$ is the macroscopic density, and $N_A$ is Avogadro's number. The motivation for the contrast variation SANS study is to determine the scattering length density of the carbon matrix. Then it becomes possible to soak the carbon powders in a solvent whose scattering length density is similar to that of the carbon matrix and thus suppress the scattering from the carbons. In principle, if the pores in the whole network are accessible to the solvent, there would not be any coherent scattering from the slurry (see eq 2). On the other hand, if some pores are not accessible to the solvent (closed pores), then the scattering signals will be strong and their shape may vary depending on the distribution of the closed porosity. The information on the closed-porosity systems will be valuable to understand the performance of the carbon in the lithium ion cells. For battery applications, if the liquid organic electrolyte penetrates the pores of the carbon anode, it leads to irreversible electrolyte decomposition during the first electrochemical reaction of lithium with the carbon, and hence a large irreversible capacity.[24] Parts a and b of Figure 4 show the contrast variation, $\sqrt{I(q)}$ at $q$ = 0.01 Å$^{-1}$, as a function of the deuteration level of toluene, for two carbon samples derived from pyrene and propylene. In this $q$ region the interface between the carbon and the pores should produce the scattering. It can be seen from Figure 4 that the contrast match points [I($q$) = 0] for the carbons derived from pyrene and propylene are 84.0% and 82.7%, respectively. These data agree well with the expected values based on the chemical composition and density of these carbons. With an elemental composition of 95.6% carbon and 5.4% hydrogen by weight, and a measured density of 2.2 g/cm$^3$ for the carbon derived from pyrene, we determine the number of carbon and hydrogen atoms per unit volume as C = 7967 and H = 4365. This corresponds to a scattering length density of 4.852 $\times$ $10^{10}$/cm$^2$, which is equivalent to that of 83.9% deuterated toluene. Similarly, for the carbon derived from propylene, the composition was 95.5% carbon and 5.5% hydrogen by weight, which corresponds to C = 7958 and H = 4464 per unit volume. The scattering length density for this carbon is 4.795 $\times$ $10^{10}$/cm$^2$, which is equivalent to that of 82.7% deuterated toluene. Thus the contrast match point for the carbon matrix is consistent with the expected values based on the elemental composition and the macroscopic density.

We then measured SANS data for the carbon powder samples derived from pyrene and from propylene, immersed in 84% toluene-$d_8$. Figure 5 shows the data

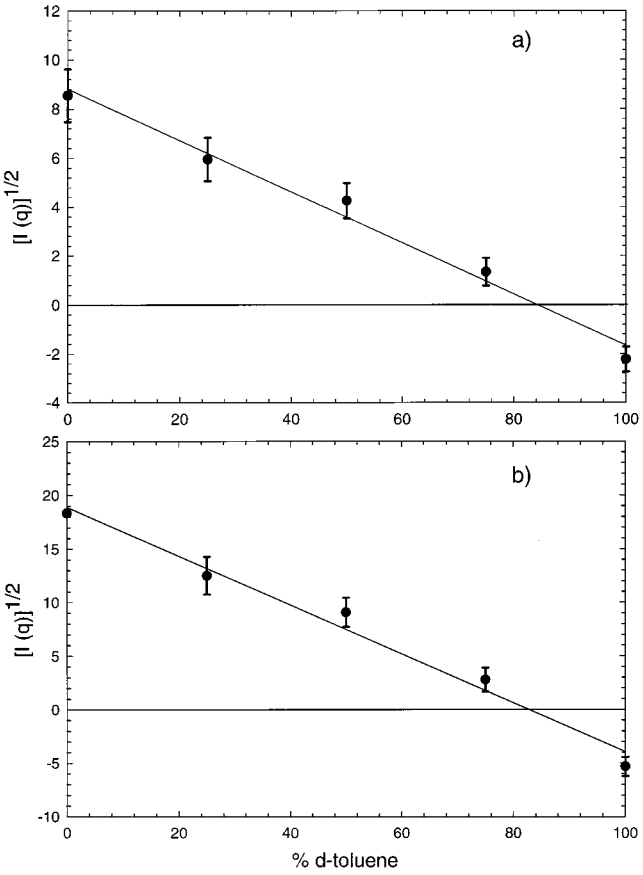


**Figure 4.** a) $\sqrt{I(q)}$ at $q$ = 0.01 Å$^{-1}$ vs the deuteration level of toluene for carbon samples derived from (a) pyrene and (b) propylene.

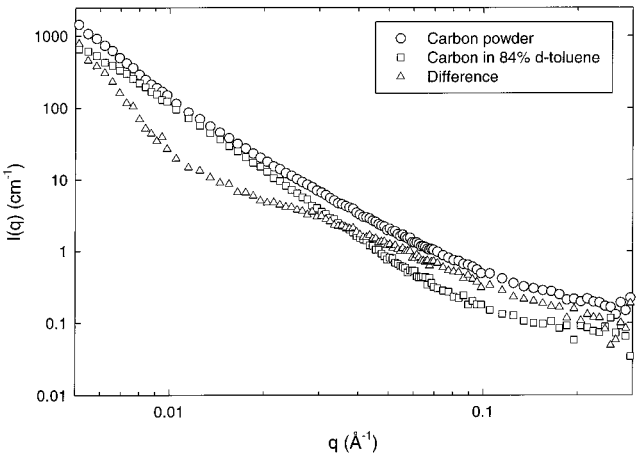


**Figure 5.** Plot of log $I$ vs log $q$ of SANS from a carbon sample derived from pyrene, the same sample in 84% toluene-$d_8$, and the difference. There is no significant reduction in the scattering intensity in the sample at contrast-matching condition for the scattering length density of carbon matrix.

for the carbon from pyrene, both as powder and immersed in the contrast matching solvent, and their difference. The scattering intensity in the low and middle $q$ regions for the carbon slurry has not significantly decreased from that for the powder, but the scattering intensity in the high $q$ region has substantially decreased. This implies that the small pores which give rise to the scattering in the high $q$ region are filled with the solvent, thus reducing the scattering signal in that region. On the other hand, the lack of reduction in

(24) Xue, J. S.; Dahn, J. R. *J. Electrochem. Soc.* **1995**, *142*, 3668.

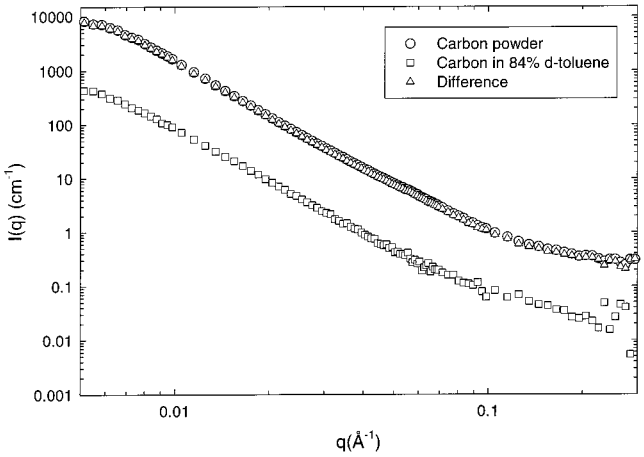


**Figure 6.** Plot of log *I* vs log *q* of SANS from a carbon sample derived from propylene, the same sample in 84% toluene-$d_8$, and the difference. In the contrast-matching solvent for the carbon, the intensity is about 20 times smaller than that for the powder.

the scattering intensity in the low and middle *q* regions indicates that a significant amount of the carbon network is not accessible to the solvent. These samples when synthesized resembled flakes which were ground to powder for the SANS determination. Analysis of the difference curve was carried on by using eq 2, but a physical picture cannot be made at this time. We believe that this requires further experiments and hence did not present the results. In contrast, the carbon from propylene seems to be quite open to the solvent, as can be seen from Figure 6, wherein the SANS data for the powder, the slurry in 84% toluene-$d_8$, and the difference are shown. The scattering intensity for this sample in 84% toluene-$d_8$ decreases by about 20 times when compared to the dry carbon sample over the entire *q* range, indicating that the porous network in this carbon has high accessibility to the solvent.

The above results on the closed porosity of carbon give clues to the better electrochemical performance of carbon derived from pyrene compared to that derived from propylene.[12] The closed porosity seems to be essential to prevent the penetration of liquid electrolytes into the bulk of the pores, so that excellent reversible behavior should be expected upon cycling the battery. Electrochemical studies of the carbons derived using inorganic templates confirm this observation.[10−12]

The BET surface areas of the carbonaceous materials range from 6 to about 85 m$^2$/g, as summarized in Table 2. Nitrogen adsorption isotherms were used to calculate

**Table 2. BET Surface Area and Average Pore Radius Based on $N_2$ Adsorption and Desorption Isotherms Obtained for the Carbon Samples**

| sample | surface area (m$^2$/g) | average pore size (Å) |
|---|---|---|
| PILC | 216 | 18.6 |
| carbon from PILC/pyrene | 6.05 | 33.3 |
| carbon from PILC/styrene | 85.0 | 20.0 |
| carbon from PILC/ethylene | 33.8 | 73.4 |
| carbon from PILC/propylene | 28.7 | 67.0 |

pore size distributions. The average pore size of the dry carbonaceous materials calculated in this way is much larger than that calculated by SANS (for example, 8 vs 67 Å in diameter for propylene). For materials where sorption is controlled by micropores, diffusion will be slow and the system cannot reach equilibrium within a reasonable time. Therefore, only those pores accessible to liquid nitrogen are considered in the calculation of surface area and the pore size distribution. Hence, one must evaluate the inaccessible micropores in carbons by using reliable techniques, such as SANS.

## Conclusions

Analysis of SANS data of carbons synthesized using clays as templates shows that they contain pores with a radius range from 4 to 11 Å. These pores are accessible to lithium ions ($Li^+$ radius for a six coordinated species is 0.9 Å[25]) when the intercalation process takes place in a lithium secondary battery. However, they are not accessible to organic solvents. This fact has important implications in the performance of lithium ion batteries, since the electrolyte decomposition is enhanced by penetration in the porous structure.

**Acknowledgment.** The help in acquiring SANS data from Mr. D. Wozniak and Dr. V. Urban, from the Intense Pulsed Neutron Source at Argonne National Laboratory, is greatly appreciated. Mr. J. Gregar, from the Chemistry Division at Argonne National Laboratory, built the physisorption cells for BET analysis and the quartz cells for the SANS experiments. This work has benefitted from the use of IPNS and was performed under the auspices of the Office of Basic Energy Sciences, Division of Chemical Sciences, U.S. Department of Energy, under contract number W-31-109-ENG-38.

CM980333J

(25) Huheey, J. E.; Keiter, E. A.; Keiter R. L. In *Inorganic Chemistry: Principles of Structure and Reactivity*, 4th ed.; Harper-Collins: New York, 1993; p 115.